

RESEARCH

Open Access



# Tyrosinase in melanoma inhibits anti-tumor activity of PD-1 deficient T cells

Rong Huang<sup>1\*†</sup>, Yingbin Wang<sup>1†</sup>, Haitao Teng<sup>1</sup>, Mengjun Xu<sup>1</sup>, Kexin He<sup>1</sup>, Yingzhuo Shen<sup>1</sup>, Guo Guo<sup>1,2</sup>, Xinyu Feng<sup>1</sup>, Tianhan Li<sup>3</sup>, Binhui Zhou<sup>4</sup>, Marc Bajenoff<sup>2,5</sup>, Toby Lawrence<sup>2,5</sup>, Yinming Liang<sup>1,6\*</sup>, Liaoxun Lu<sup>1\*</sup> and Lichen Zhang<sup>1,6\*</sup>

## Abstract

**Background** Melanoma is one of the most commonly diagnosed malignancies and serves as a model for studying immunotherapy. The B16 melanoma model, resembling human cold tumors that lack T cell infiltration and show minimal response to PD-1 blockade, is widely used for studying melanoma and its resistance to immunotherapy. Therefore, understanding the molecular basis that prevents T cell-mediated anti-tumor activity in B16 melanoma is of great significance.

**Results** In this study, we generated tyrosinase knockout B16 melanoma cells using CRISPR/Cas9 and discovered that tyrosinase in melanoma significantly inhibits the anti-tumor activity of T cells. Tyrosinase deficiency leads to a 3.80-fold increase in T-cell infiltration and enhances T-cell activation within the tumor. Single-cell RNA sequencing reveals an altered cold tumor immunophenotype in tyrosinase-deficient B16 melanoma. In wild-type mice, T cells in tyrosinase-deficient tumors express elevated levels of PD-1 and Foxp3. However, strikingly, in PD-1 deficient mice, the loss of tyrosinase in B16 melanoma unleashes the anti-tumor activity of PD-1 deficient T cells. This enhanced anti-tumor activity is explained by significantly increased tumor T cell infiltration accompanied by reduced frequencies of regulatory T cells in PD-1 knockout mice.

**Conclusions** These findings suggest that targeting tyrosinase could convert cold tumors into an immune-responsive state in vivo using murine models. Inhibiting tyrosinase could enhance the effectiveness of PD-1 blockade, offering a new approach for melanoma patients who fail in current PD-1 inhibitor treatment.

**Keywords** Melanoma, Tyrosinase, Tumor infiltrating T cells, PD-1

<sup>†</sup>Rong Huang and Yingbin Wang contributed equally to this work.

\*Correspondence:

Rong Huang  
huangrong@gris.org.cn  
Yinming Liang  
yinming.liang@foxmail.com  
Liaoxun Lu  
luliaoxun@gris.org.cn  
Lichen Zhang  
zhanglichen@gris.org.cn

<sup>1</sup> Laboratory of Genetic Regulators in the Immune System, School of Medical Technology, Xinxiang Medical University, Xinxiang, China

<sup>2</sup> Centre d'immunologie de Marseille-Luminy, Aix-Marseille University, CNRS, INSERM, Marseille, France

<sup>3</sup> School of Basic Medical Sciences, Xinxiang Medical University, Xinxiang, China

<sup>4</sup> Institute of Psychiatry and Neuroscience, Xinxiang Medical University, Xinxiang, China

<sup>5</sup> Centre for Inflammation Biology and Cancer Immunology, School of Immunology & Microbial Sciences, King's College London, London, UK

<sup>6</sup> Center of Disease Model and Immunology, Hunan Academy of Chinese Medicine, Changsha, China



## Background

Melanoma, an aggressive and dangerous form of skin cancer, arises from the transformation of melanocytes, the pigment-forming cells of the skin. Previous studies have established that pigmentation influences the prognosis and treatment response in melanoma. Melanin pigmentation has been associated with reduced overall survival and disease-free survival in patients with advanced melanoma stages [1]. The enzyme tyrosinase (Tyr) plays a pivotal role in initiating melanin synthesis within melanosomes. Previous genome-wide association studies have identified associations between tyrosinase genetic loci and melanoma risk, suggesting a link with pigmentation-related genes [2]. Notably, reducing systemic tyrosine levels has been shown to impede melanoma growth both in vitro and in vivo [3–5]. However, the underlying mechanisms of melanin synthesis in cancer progression have not yet been elucidated.

In recent years, checkpoint inhibition immunotherapy, particularly PD-1/PD-L1 blockades, has emerged as one of the most successful strategies for cancer treatment, functioning through the stimulation of the patient's immune system [6–9]. Although promising results from early clinical trials suggest that anti-PD-1 therapy extends survival among the current melanoma therapeutic agents [10, 11], the efficacy of anti-PD-1 therapy remains variable, particularly in patients with tumors demonstrating low T cell infiltration and an immune-excluded phenotype [12, 13]. Therefore, a combination of complementary therapeutic strategies may have a better chance of success.

The B16 mouse melanoma model is highly immunosuppressive, with an immune-excluded tumor microenvironment (TME) characterized by low T cell infiltration, and blockade of the PD-1 pathway has no evident anti-tumor activity, resembling the cold-tumor immunophenotype observed in melanoma patients. Previous studies indicated that the efficacy of PD-1 blockade was largely confined to patients with tumors that have robust baseline T cell infiltrates [14, 15]. In our study, we utilized the CRISPR/Cas9 system to generate tyrosinase knockout (KO) B16 melanoma cells and discovered that tyrosinase significantly inhibits the anti-tumor activity of T cells in melanoma. Single-cell RNA sequencing (scRNA-seq) and flow cytometry analyses revealed an altered cold-tumor immunophenotype in tyrosinase-deficient B16 melanoma, characterized by increased T cell infiltration and activation within the tumor microenvironment. Remarkably, the T cells infiltrating tyrosinase-deficient tumors exhibited an exaggerated expression of PD-1 and Foxp3, which are critical markers associated with T cell

exhaustion and regulatory T cell function, respectively. Our further research showed that the loss of tyrosinase in B16 melanoma enhances the anti-tumor potential of PD-1-deficient T cells, as evidenced by increased tumor T cell infiltration and reduced regulatory T cell (Treg) frequencies in PD-1 knockout mice.

Collectively, our study provides compelling evidence that tyrosinase in melanoma plays a crucial role in inhibiting the anti-tumor activity of PD-1-deficient T cells, revealing a novel mechanism by which tyrosinase contributes to the suppression of anti-tumor immunity in cold tumors with an immune-excluded microenvironment. Targeting tyrosinase in melanoma could enhance the anti-tumor response when T cell exhaustion from PD-1 is blocked, providing a promising target for immunotherapy.

## Results

### Generation of Tyr knockout B16 melanoma cells by CRISPR/Cas9

Tyrosinase plays a critical role in regulating the early stages of melanin synthesis by catalyzing the initial two steps in melanin biosynthesis, which involve the ortho-hydroxylation of L-tyrosine and the oxidation of L-DOPA [16]. However, its implication in cancer progression and prognosis has not been elucidated. Analysis of data from The Cancer Genome Atlas (TCGA) reveals elevated Tyr expression in Skin Cutaneous Melanoma (SKCM) tumor samples compared to normal skins, indicating an evident involvement of Tyr in SKCM in humans (Fig. 1A). An important finding is the correlation between high Tyr expression and reduced overall survival in SKCM patients ( $p < 0.05$ ) (Fig. 1B), suggesting the potential of Tyr as a prognostic marker for the disease. In our study, CRISPR/Cas9 technology was employed to disrupt the *Tyr* gene in B16-F10 melanoma cells, a well-established murine melanoma cell line. Guide RNAs were specifically designed to target exon 1 of the mouse *Tyr* gene (ENSMUST00000004770.6) (Fig. 1C). Plasmids containing the Cas9 nuclease and single guide RNAs (sgRNAs) were introduced into cells along with two fluorescent reporters, ECFP and DsRed2, to aid in the identification and sorting of successfully edited cells as described in the Material and Methods section. Mutant clones were isolated and validated by PCR and three independent clones were used for further experiments, namely C1, C2 and C3 (Fig. 1D). Sanger sequencing further validated deletions of *Tyr* gene which affected the protein coding sequence in three distinct clones (Additional file 1: Fig. S1). A remarkably visible result from the *Tyr* gene knockout is an obvious change in pigmentation of the B16-F10 cells, indicating disruption of melanin synthesis (Fig. 1E).

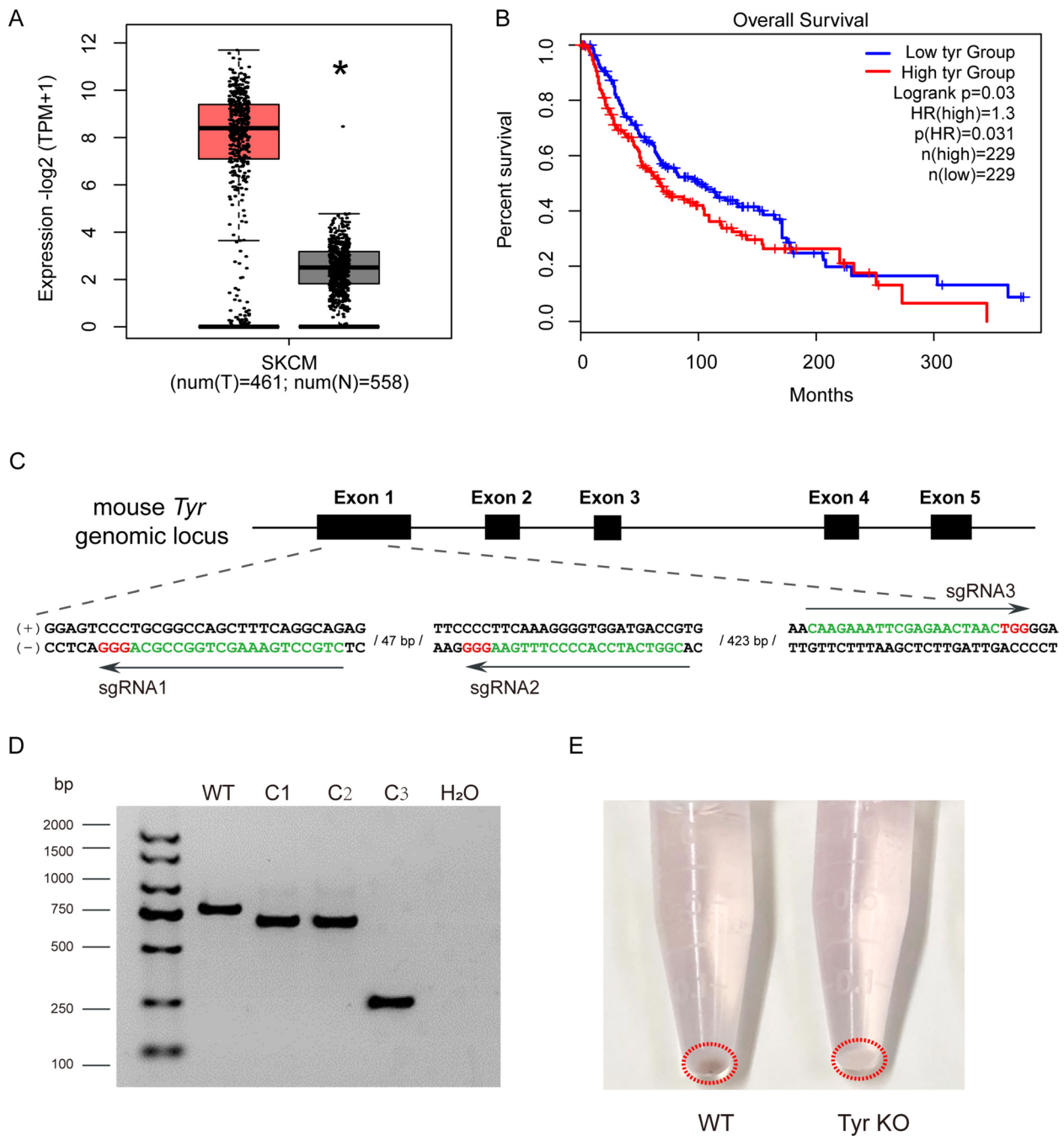


**Fig. 1** Generation of *Tyr* knockout B16 melanoma cells by CRISPR/Cas9. **A** Elevated *Tyr* expression in SKCM tumor tissues compared to normal tissues. The data were obtained from the GEPIA2 database (<http://gepia2.cancer-pku.cn>). T: SKCM tumor tissues, N: Normal tissues. ( $*p < 0.05$ ). **B** Analysis of the correlation between *Tyr* expression and clinical prognosis in SKCM patients, indicated by overall survival rates from the GEPIA2 database. **C** Illustration of sgRNA sequences targeting *Tyr* gene in B16-F10 cells. A visual depiction of the three guide RNA sequences designed to target exon 1 of the *Tyr* gene in B16-F10 cells is presented in this schematic. The protospacer adjacent motifs (PAMs) are highlighted in red. **D** Identification of *Tyr* knockout clones in B16-F10 cells through PCR screening. The three deletion clones are identified as C1, C2, and C3. M referred to the DNA size marker, WT referred to the wild-type B16-F10 control, and H<sub>2</sub>O was used as a negative control for PCR amplification. **E** Visual comparison of pigmentation in wild-type (WT) and *Tyr* knockout (KO) B16-F10 cells

### Tyrosinase deficiency turns B16 melanoma from cold-tumor into hot-tumor

Using the Tyr KO cells, we first aimed to evaluate the effects of Tyr deficiency on tumor progression by grafting wild-type (WT) B16-F10 and Tyr<sup>-/-</sup> B16-F10 cells to genetically identical C57BL/6 (B6) mice. After fourteen days, we observed a change in the pigmentation of tumors grown from the mixture of three Tyr KO clones (Fig. 2A), which was consistent with the in vitro cell line findings (Fig. 1E). Additionally, the Tyr<sup>-/-</sup> B16-F10 cells exhibited a significantly reduced tumor mass compared to the WT cells (Fig. 2B). To further explore the impact of Tyr KO on the TME, we used single-cell RNA sequencing to analyze sorted CD45<sup>+</sup> cells in tumors from WT or KO melanoma (Additional file 1: Fig. S2). CD45<sup>+</sup> tumor-infiltrating immune cells were isolated and analyzed using BD Rhapsody scRNA-seq technology. A total of 8,658 cells (4,198 in KO and 4,460 in WT cells) from pooled samples of three mice in each group were analyzed using SeqGeq.

Our analysis identified 14 distinct cellular clusters within the tumors, including macrophages (cluster 1–4), CD4<sup>+</sup> T cells (cluster 5), neutrophils (cluster 6), conventional dendritic cells (cDCs, cluster 7), natural killer cells (NK, cluster 8), granulocytes (cluster 9), CD8<sup>+</sup> T cells (cluster 10), B cells (cluster 11), dendritic cells (DCs, cluster 12), tumor cells (cluster 13), and plasmacytoid dendritic cells (pDCs, cluster 14) (Fig. 2C, Additional file 1: Fig. S3). Notably, tumors derived from Tyr<sup>-/-</sup> B16-F10 cells exhibited distinct immune cell infiltration compared to those derived from WT B16-F10 cells, characteristic of an increase in CD4<sup>+</sup> and CD8<sup>+</sup> T cells (Fig. 2D). We also conducted flow cytometry analysis to validate the findings from scRNA-seq (Fig. 2E), and found a significantly higher number of CD45<sup>+</sup> immune cells within Tyr<sup>-/-</sup> B16-F10 tumors (Fig. 2F). In Tyr<sup>-/-</sup> B16-F10 tumors, T cells made up 12.08% of all tumor-infiltrating immune cells, totaling 1.72 million T cells per gram of tissue, 3.80-fold higher than T cell numbers in WT B16-F10 tumors (Fig. 2G, I). Additionally, the cell numbers of both CD4<sup>+</sup> and CD8<sup>+</sup> T cells also increased significantly in Tyr<sup>-/-</sup> tumors (Fig. 2I), while the overall percentages and the cell numbers of CD11b<sup>+</sup> remained unaffected (Fig. 2H, J). Our findings validate that the deficiency of tyrosinase in B16-F10 melanoma led to a reduction in tumor weight and changes in immune cell infiltration, notably an increase in T cells within the tumor. Our research indicates that tyrosinase exerts a notable impact on the TME, particularly in converting “cold tumors” into a more immune-responsive state.

### Tyrosinase in B16 melanoma prevents expression of PD-1 and Foxp3 in tumor infiltrating T cells

After observing a notable rise in the quantity of T cells in tyrosinase-deficient tumors in comparison to controls, we proceeded to analyze the immune checkpoint molecules on T cells within the tumors. As shown in Fig. 3A, we analyzed the T-cell phenotype in Tyr<sup>-/-</sup> tumors and WT controls. Notably, tyrosinase deficiency in tumor increases the expression of PD-1 in both CD4<sup>+</sup> and CD8<sup>+</sup> T cells, with a more dramatic increase in CD8<sup>+</sup> T cells from 25.67% to 47.22% (Fig. 3B, C). In the Tyr<sup>-/-</sup> tumors, the flow cytometric analysis revealed a higher percentage of CTLA-4<sup>+</sup> cells in both CD4<sup>+</sup> and CD8<sup>+</sup> T cell populations, compared to the WT tumors (Fig. 3D, E). Considering the dominant roles of Tregs in immune tolerance, we subsequently analyzed the Tregs in Tyr<sup>-/-</sup> and WT tumors. Strikingly, the average frequency of Foxp3<sup>+</sup> cells was 29.46% in CD4<sup>+</sup> T cells, representing a 2.24-fold increase in Tregs in Tyr<sup>-/-</sup> tumors compared to WT controls (Fig. 3F). Tyrosinase deficiency increases numbers of tumor infiltrating T cells, and increases expression of PD-1 and CTLA-4, which therefore targeting of tyrosinase may strengthen the therapeutic efficacy when blockade of immune checkpoint molecules is applied.

### Tyrosinase deficiency significantly increases production of effector cytokines in tumor infiltrating T cells

Data above show elevated numbers of tumor infiltrating T cells and PD-1 expression in tyrosinase-deficient tumors. To gain a deeper understanding of the transcription factor and cytokine response program in these tumors, we performed Quantitative real-time PCR (q-PCR) analysis on total mRNAs extracted from tumor to quantify the expression levels of hallmark genes. The gene expression data illustrated upregulation of Tbx21, Nr4a1, TNF- $\alpha$  and IFN- $\gamma$  in tyrosinase-deficient tumors, as depicted in Fig. 4A. Nr4a1 is a key transcription factor that dominates expression of PD-1 [17, 18], and our finding that Nr4a1 mRNA displayed 1.79-fold increase in tyrosinase-deficient tumors was in line with the significantly elevated co-inhibitory molecule PD-1. The effector cytokines IFN- $\gamma$  and TNF- $\alpha$ , crucial in T cell responses against tumor [19], exhibited over a 15-fold increase in tyrosinase-deficient tumors. Tbx21, a master transcription factor governing IFN- $\gamma$  production [20], was 15.51-fold higher in Tyr<sup>-/-</sup> tumors compared to WT tumors.

Furthermore, we analyzed the gene expression profiles of T cells corresponding to Cluster 5 and Cluster 10 in Tyr<sup>-/-</sup> and control tumors using scRNA-seq data as described above. T cells were visualized based on CD3 expression in the *t*-SNE cluster map generated by Seurat through unsupervised clustering analysis, which included

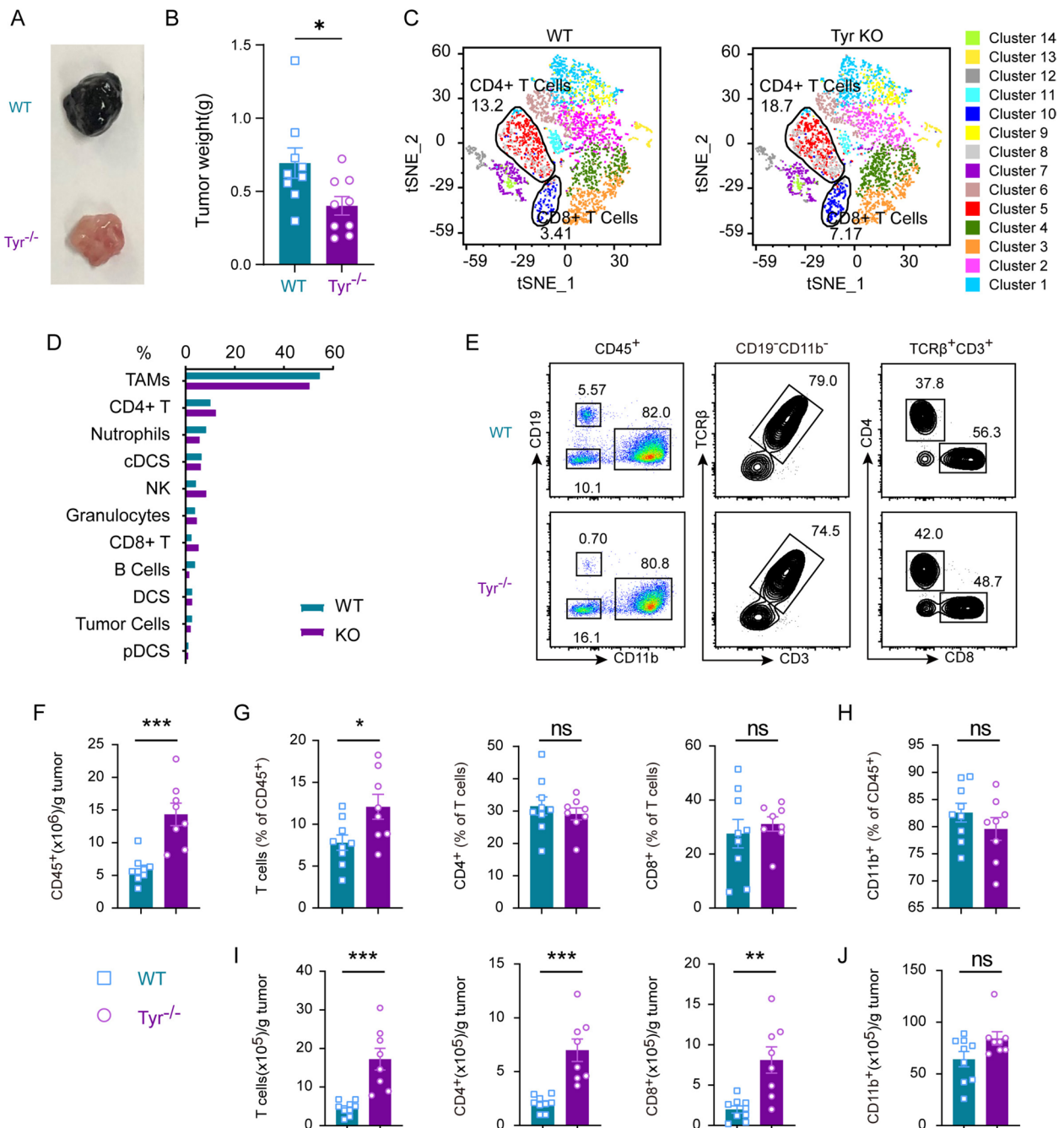


**Fig. 2** Characterization of tumor-infiltrating immune cells in WT and Tyr<sup>-/-</sup> B16-F10 melanoma model. **A** Representative images of WT and Tyr<sup>-/-</sup> B16-F10 tumors from female C57BL/6 mice on day 14. **B** The weight of WT and Tyr<sup>-/-</sup> B16-F10 tumors on day 14. **C** The immune infiltration profiling in WT and Tyr<sup>-/-</sup> B16-F10 tumors through scRNA-Seq. CD4<sup>+</sup> immune cells from WT and Tyr<sup>-/-</sup> B16-F10 tumors were sorted and analyzed. Pooled samples from three mice per group were used. Dimensionality reduction was done with the t-SNE algorithm and cell clustering using Seurat. Each cluster was denoted a unique color. t-SNE, t-distributed stochastic neighbor embedding. **D** Proportions of different immune cell types in WT and Tyr<sup>-/-</sup> B16-F10 tumors. **E** Gating strategy for tumor-infiltrating immune cells, including CD11b<sup>+</sup> cells and T cells, in WT and Tyr<sup>-/-</sup> B16-F10 tumors. Cells were gated based on CD45<sup>+</sup>, CD11b<sup>+</sup>, CD19<sup>+</sup>, CD3<sup>+</sup> TCRβ<sup>+</sup>, CD4<sup>+</sup>, and CD8<sup>+</sup> markers. **F** Quantification of tumor-infiltrating CD45<sup>+</sup> cells in WT and Tyr<sup>-/-</sup> B16-F10 tumors. **G** The proportion of T cells, CD4<sup>+</sup> T cells and CD8<sup>+</sup> T cells among tumor-infiltrating CD45<sup>+</sup> cells in WT and Tyr<sup>-/-</sup> B16-F10 tumors. **H** Proportion of CD11b<sup>+</sup> cells among tumor-infiltrating CD45<sup>+</sup> cells in WT and Tyr<sup>-/-</sup> B16-F10 tumors. **I–J** Cell counts of T cells, CD4<sup>+</sup> T cells, CD8<sup>+</sup> T cells (I), and CD11b<sup>+</sup> cells (J) per gram of tissue in WT and Tyr<sup>-/-</sup> B16-F10 tumors. Data are presented as mean ± SEM (WT tumors, n = 9; Tyr<sup>-/-</sup> tumors, n = 8 or 9). All data are pooled from two independent experiments. Statistical significances were calculated using Student’s t-test (\* p < 0.05; \*\* p < 0.01; \*\*\* p < 0.001; ns, not significant)

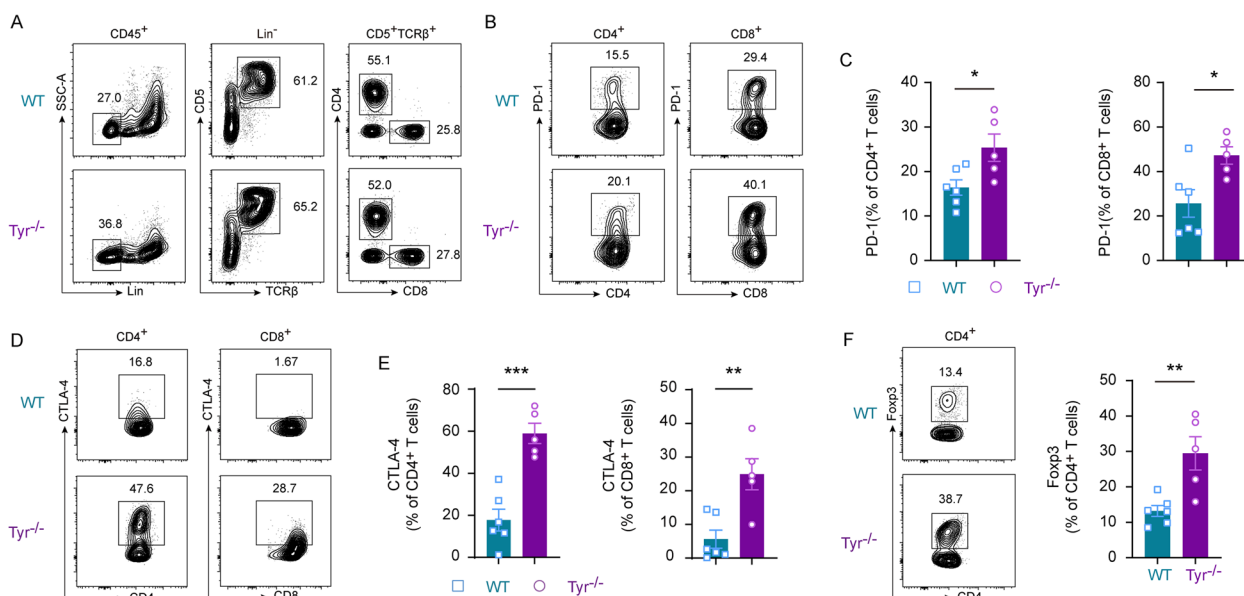


**Fig. 3** Enhanced PD-1 and Foxp3 expression in tyrosinase-deficient tumors T Cells. **A–B** Flow cytometric analysis of PD-1 expression in WT and Tyr<sup>-/-</sup> tumors. Cells were firstly gated on CD45<sup>+</sup> and Lin<sup>-</sup> (CD19, CD11b, NK1.1, Ly6G), then further gated on CD5<sup>+</sup> TCRβ<sup>+</sup>, CD4<sup>+</sup>, and CD8<sup>+</sup> cells. **C** Percentage of PD-1<sup>+</sup> cells within CD4<sup>+</sup> and CD8<sup>+</sup> T cells in WT and Tyr<sup>-/-</sup> B16-F10 tumors. **D–E** Flow cytometric analysis of PD-1 expression in WT and Tyr<sup>-/-</sup> tumors. Proportion of CTLA-4<sup>+</sup> cells within CD4<sup>+</sup> and CD8<sup>+</sup> T cells in WT and Tyr<sup>-/-</sup> B16-F10 tumors (**E**). **F** Flow cytometric analysis of Foxp3 expression in WT and Tyr<sup>-/-</sup> tumors. Histograms on the right show the proportion of Foxp3 in CD4<sup>+</sup> T cells in WT and Tyr<sup>-/-</sup> tumors. Data are presented as mean ± SEM (WT tumors, n = 6; Tyr<sup>-/-</sup> tumors, n = 5). All data are representative of two independent experiments. Statistical significances were calculated using Student's t-test (\* p < 0.05; \*\* p < 0.01; \*\*\* p < 0.001)

gated CD4<sup>+</sup> and CD8<sup>+</sup> T cell populations (Figs. 2C and 4B). Marker genes for CD4 (cluster 5) and CD8 (cluster 10) are listed in the supplementary file (Additional file 1: Fig. S3). In CD4<sup>+</sup> T cells, Tyr<sup>-/-</sup> tumors exhibited increased expression of the transcription factors Nr4a1, Tbx21, and IL-2, with no obvious differences in TNF-α and IFN-γ expression compared to control tumors (Fig. 4C). We did not find obvious changes in expression of such genes in CD8<sup>+</sup> T cells (Fig. 4D), which is probably due to the scarcity of CD8<sup>+</sup> T cells analyzed. Our findings demonstrate that tyrosinase-deficient tumors exhibit elevated levels of T cells and PD-1 expression, along with upregulation of key transcription factors and cytokines involved in T cell responses. At single-cell level, we found in CD4<sup>+</sup> T cells increased expression of Nr4a1, Tbx21, and IL-2 in tyrosinase-deficient tumors.

To investigate the direct interaction between tyrosinase sufficient and deficient melanoma cells and T cells, we performed in vitro co-culture assays. T cells were

co-cultured with B16-F10 cells, including WT, Tyr KO, and Tyr knock-in (KI) cells which was a genetic rescue on the background of tyrosinase knockout and resulted in fully restored tyrosinase expression in Tyr-deficient B16-F10 melanoma cells (Additional file 1: Fig. S4). Remarkably, q-PCR analysis revealed that Tyr KO cells induced 1.62 to 2.65-fold higher expression of Tbx21, Nr4a1, TNF-α and IFN-γ in T cells compared to WT controls, but strikingly such effects were totally abolished in the Tyr KI cells (Additional file 1: Fig. S5). These findings suggest that tyrosinase is critical in suppressed T cell activation.

### Loss of tyrosinase in B16 melanoma unleashes T cell-mediated tumor immunity of PD-1 deficient mice

In both animal models and human patients, the therapeutic effects of immune checkpoint molecule blockade depend on the levels of these molecules expressed by T cells. In our study, we observed that tyrosinase deficiency

(See figure on next page.)

**Fig. 4** Altered cold-tumor immunophenotype revealed by single-cell RNA sequencing in tyrosinase-deficient B16 melanoma. **A** q-PCR analyses of Tbx21, Nr4a1, TNF-α and IFN-γ mRNAs in WT and Tyr<sup>-/-</sup> B16-F10 tumors (WT tumors, n = 5; Tyr<sup>-/-</sup> tumors, n = 5). Each point represents the mean value obtained from two replicates for an individual mouse. Statistical significances were calculated using Student's t-test (\* p < 0.05; \*\* p < 0.01). **B** The expression levels and distribution of CD3 in WT and Tyr<sup>-/-</sup> tumors demonstrated by t-SNE. **C** t-SNE visualization of the expression of IL-2, Tbx21, Nr4a1, TNF-α, and IFN-γ in CD4 cells (cluster 5). **D** t-SNE visualization of the expression of IL-2, Tbx21, Nr4a1, TNF-α, and IFN-γ in CD8 cells (cluster 10)

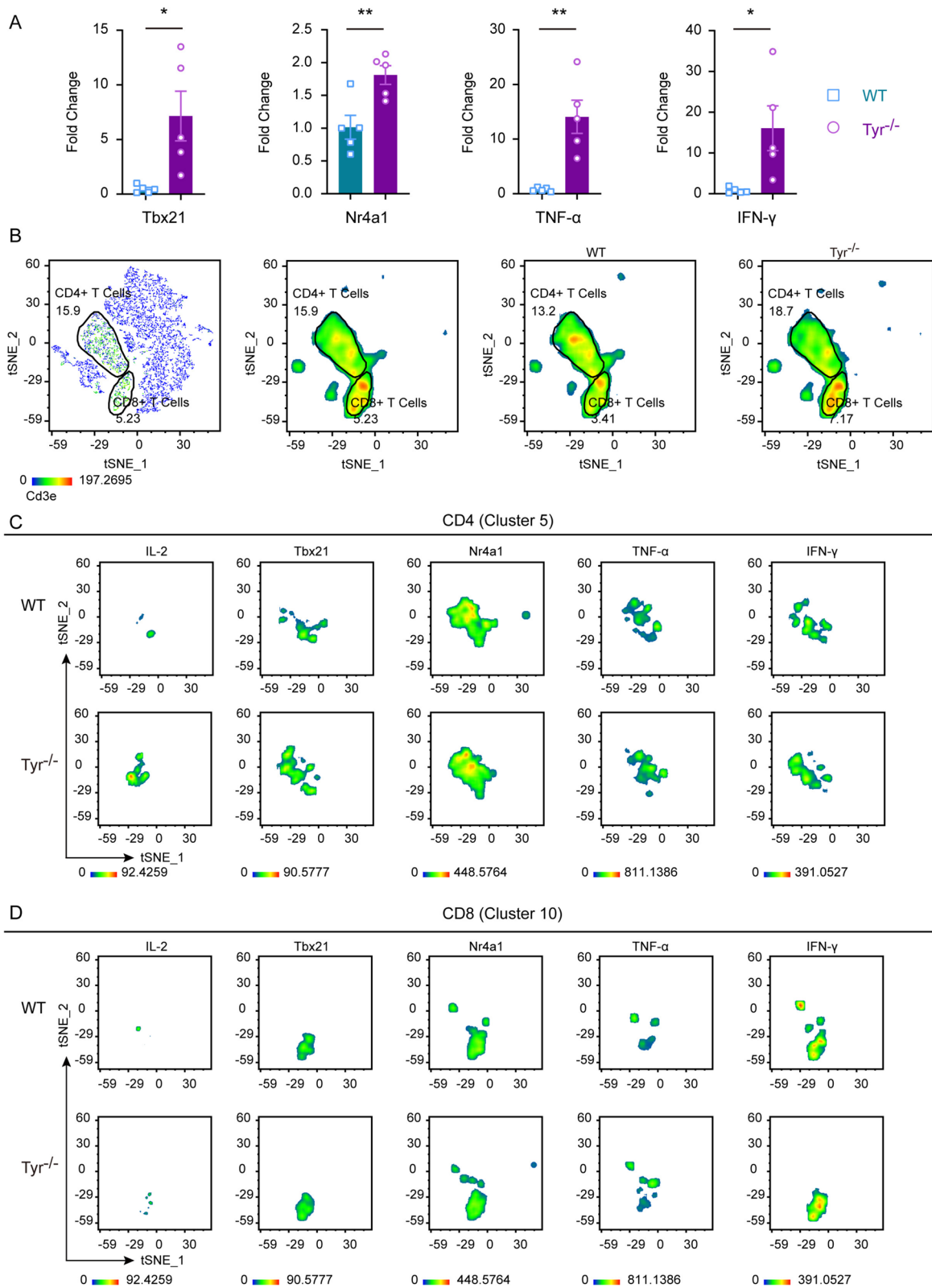


**Fig. 4** (See legend on previous page.)

led to elevated T cell numbers and elevated PD-1 expression in CD4<sup>+</sup> and CD8<sup>+</sup> T cells. The primary objective of our research was to investigate whether loss of tyrosinase could unleash T cell-mediated tumor immunity of PD-1 deficient mice. *Pdcd1*-deficient C57BL/6 mice were generated using CRISPR/Cas9 targeting the *Pdcd1* gene and the knockout mice were validated by loss of surface PD-1 expression in FACS experiments, as described in our previous study [21].

Subcutaneous injection of tyrosinase sufficient Tyr<sup>+/+</sup> B16-F10 melanoma cells into syngeneic C57BL/6 WT mice and B6 *Pdcd1*<sup>-/-</sup> mice led to the formation of largely comparable tumor weight in both groups of mice (Fig. 5A). Further analysis of tumor-infiltrating immune cells showed no significant differences in cell numbers of T cells within the tumors of *Pdcd1*<sup>-/-</sup> mice compared to the B6 WT controls (Fig. 5B). Additionally, the numbers of CD45<sup>+</sup> cells, including CD4<sup>+</sup> and CD8<sup>+</sup> T cells, remained unchanged (Additional file 1: Fig. S6). Our results were consistent with findings from previous studies [22–24]. In our study, we did not observe

any significant changes in the frequencies of CTLA-4 (Fig. 5C, D) and Foxp3 (Fig. 5E, F) expressing T cells in tumor, when we compared B6 WT mice and PD-1 knockout mice following engraftment of tyrosinase sufficient B16-F10 tumor cells.

In tyrosinase-sufficient Tyr<sup>+/+</sup> tumors, T cells in *Pdcd1*<sup>-/-</sup> mice did not demonstrate improved ability to inhibit tumor growth compared to B6 WT mice. Hence, it was of interest to investigate if tyrosinase deficiency could unleash the anti-tumor potential of *Pdcd1*<sup>-/-</sup> T cells. Tyr<sup>-/-</sup> B16-F10 cells transplanted subcutaneously into both *Pdcd1*<sup>-/-</sup> mice and B6 WT control mice. Interestingly we first found that the weight of Tyr<sup>-/-</sup> tumor was significantly reduced in *Pdcd1*<sup>-/-</sup> mice compared to the B6 controls (Fig. 6A). This reduction was associated with a significant increase in T cell infiltration (Fig. 6B, Additional file 1: Fig. S7), indicating that tyrosinase deficiency was able to boost T cell response in *Pdcd1*<sup>-/-</sup> mice. Analysis of tumor-infiltrating T cells showed a significant decrease of CTLA-4 expressing CD4<sup>+</sup> T cells in tumors from *Pdcd1*<sup>-/-</sup> mice compared with B6 mice (Fig. 6C,

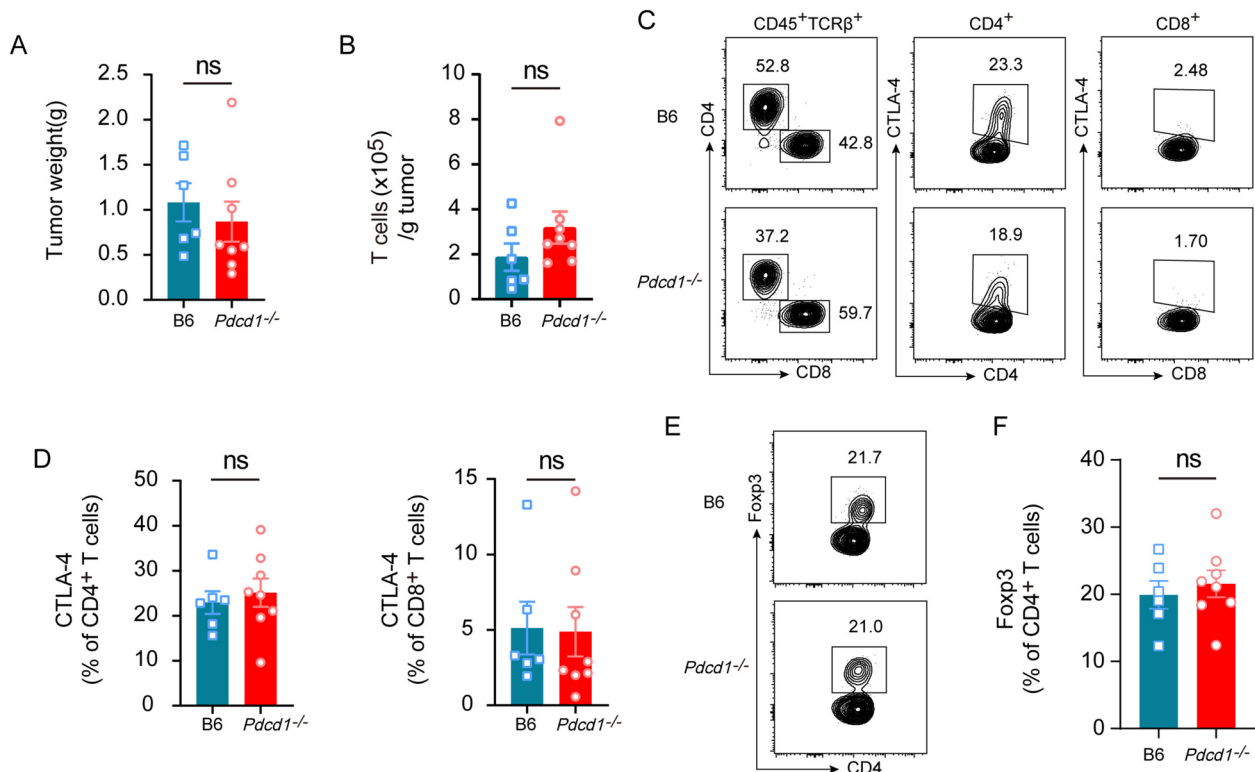


**Fig. 5** The effects of PD-1 blockade on tumor growth and T cells in Tyr<sup>+/+</sup> B16-F10 tumors. **A** The tumor weight of Tyr<sup>+/+</sup> B16-F10 cell grafted *Pdcd1*<sup>-/-</sup> and B6 mice. **B** Quantification of tumor-infiltrating T cells by flow cytometry in Tyr<sup>+/+</sup> B16-F10 tumors from *Pdcd1*<sup>-/-</sup> and B6 mice. **C** Representative flow cytometry analysis of CTLA-4<sup>+</sup> cells in Tyr<sup>+/+</sup> B16-F10 tumors from *Pdcd1*<sup>-/-</sup> and B6 mice. Cells were identified based on CD45<sup>+</sup>, TCR-β<sup>+</sup>, CD4<sup>+</sup>, and CD8<sup>+</sup> markers. **D** Quantification of the frequency of CTLA-4<sup>+</sup> cells within CD4<sup>+</sup> and CD8<sup>+</sup> T cells in Tyr<sup>+/+</sup> B16-F10 tumors from *Pdcd1*<sup>-/-</sup> and B6 mice. **E–F** Flow cytometric analysis of Foxp3 expression in Tyr<sup>+/+</sup> B16-F10 tumors from *Pdcd1*<sup>-/-</sup> and B6 mice. Proportion of Foxp3 in CD4<sup>+</sup> T cells of Tyr<sup>+/+</sup> B16-F10 tumors from *Pdcd1*<sup>-/-</sup> and B6 mice (**F**). Data are presented as mean ± SEM (B6 mice, n = 6; *Pdcd1*<sup>-/-</sup> mice, n = 8). Statistical significances were calculated using Student's t-test (ns, not significant)

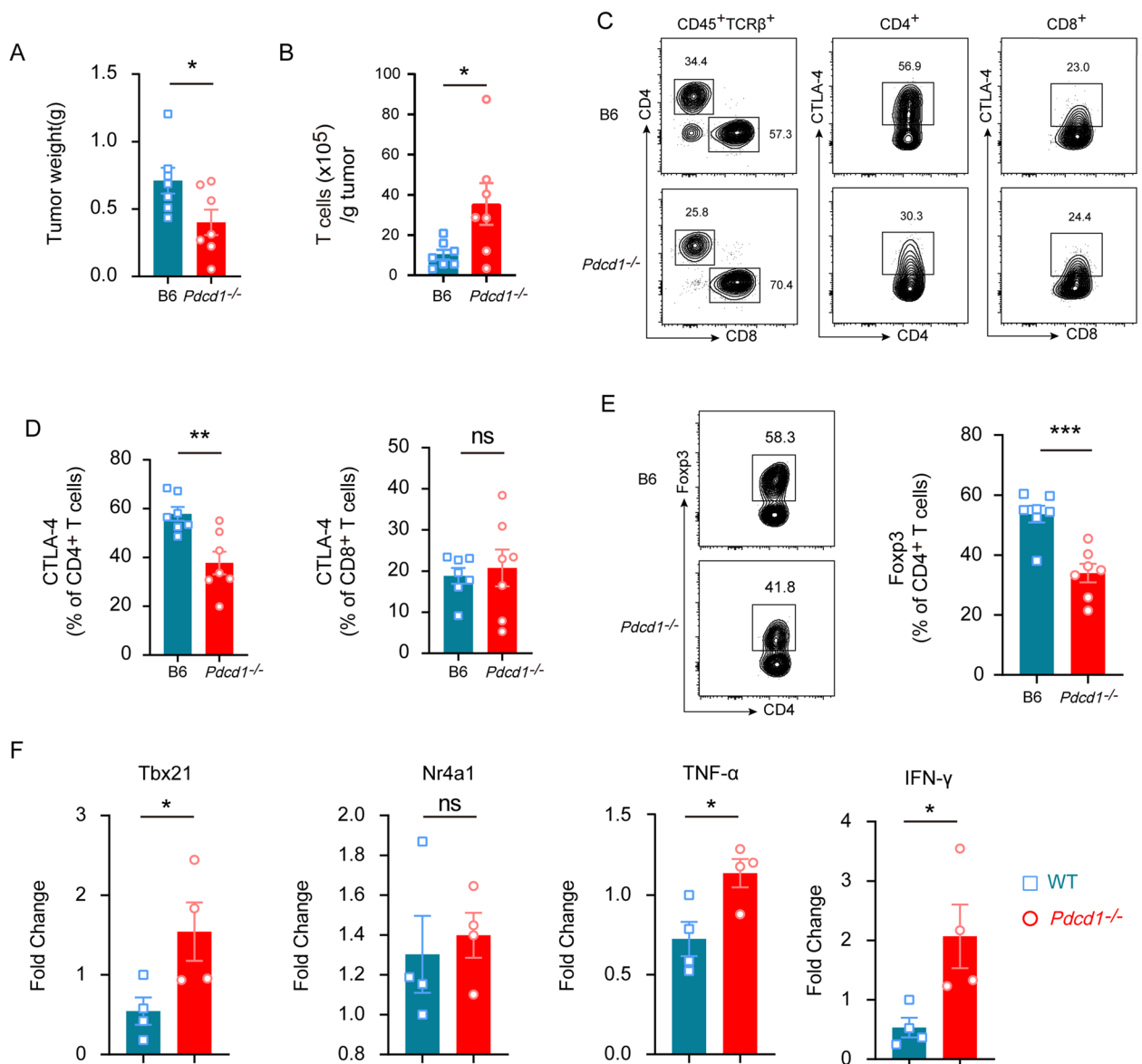


**Fig. 6** Loss of tyrosinase in B16 melanoma unleashes T cell-mediated tumor immunity of PD-1 deficient mice. **A** The tumor weight of *Tyr*<sup>-/-</sup> B16-F10 cell grafted *Pdc1*<sup>-/-</sup> and B6 mice. **B** Quantification of tumor-infiltrating T cells by flow cytometry in *Tyr*<sup>-/-</sup> B16-F10 tumors from *Pdc1*<sup>-/-</sup> and B6 mice. **C** Representative flow cytometry analysis of CTLA-4<sup>+</sup> cells in *Tyr*<sup>-/-</sup> B16-F10 tumors from *Pdc1*<sup>-/-</sup> and B6 mice. Cells were identified based on CD45<sup>+</sup>, TCR-β<sup>+</sup>, CD4<sup>+</sup>, and CD8<sup>+</sup> markers. **D** Quantification of the frequency of CTLA-4<sup>+</sup> cells within CD4<sup>+</sup> and CD8<sup>+</sup> T cells in *Tyr*<sup>-/-</sup> B16-F10 tumors from *Pdc1*<sup>-/-</sup> and B6 mice. **E** Flow cytometric analysis of Foxp3 expression in *Tyr*<sup>-/-</sup> B16-F10 tumors from *Pdc1*<sup>-/-</sup> and B6 mice. Proportion of Foxp3 in CD4<sup>+</sup> T cells of *Tyr*<sup>-/-</sup> B16-F10 tumors from *Pdc1*<sup>-/-</sup> and B6 mice. **F** q-PCR analyses of *Tbx21*, *Nr4a1*, *TNF-α* and *IFN-γ* mRNAs in *Tyr*<sup>-/-</sup> B16-F10 tumors from *Pdc1*<sup>-/-</sup> and B6 mice (WT tumors, *n* = 4; *Tyr*<sup>-/-</sup> tumors, *n* = 4). Each point represents the mean value obtained from two replicates for an individual mouse. Data in 6A-E are presented as mean ± SEM (B6 mice, *n* = 7; *Pdc1*<sup>-/-</sup> mice, *n* = 7), representative of two independent experiments. Statistical significances were calculated using Student's *t*-test (\* *p* < 0.05; \*\* *p* < 0.01; \*\*\* *p* < 0.001; ns, not significant)

D). Surprisingly, in *Tyr*<sup>-/-</sup> tumor, there was a notable decrease in Foxp3<sup>+</sup> Tregs in *Pdc1*<sup>-/-</sup> mice compared with B6 controls (Fig. 6E). Furthermore, elevated expression of *Tbx21*, *TNF-α*, and *IFN-γ* was found in *Pdc1*<sup>-/-</sup> mice (Fig. 6F). From our experiments comparing T cell response in *Pdc1*<sup>-/-</sup> and WT mice using *Tyr*<sup>-/-</sup> tumor,

we found that tyrosinase deficiency could unleash the anti-tumor potential of *Pdc1*<sup>-/-</sup> T cells (Fig. 7).

To directly assess the impact of tyrosinase deficiency on anti-PD-1 therapy, we performed in vivo PD-1 blockade experiments using anti-PD-1 antibodies in mice bearing WT and *Tyr*<sup>-/-</sup> B16-F10 tumors. In WT tumors, PD-1

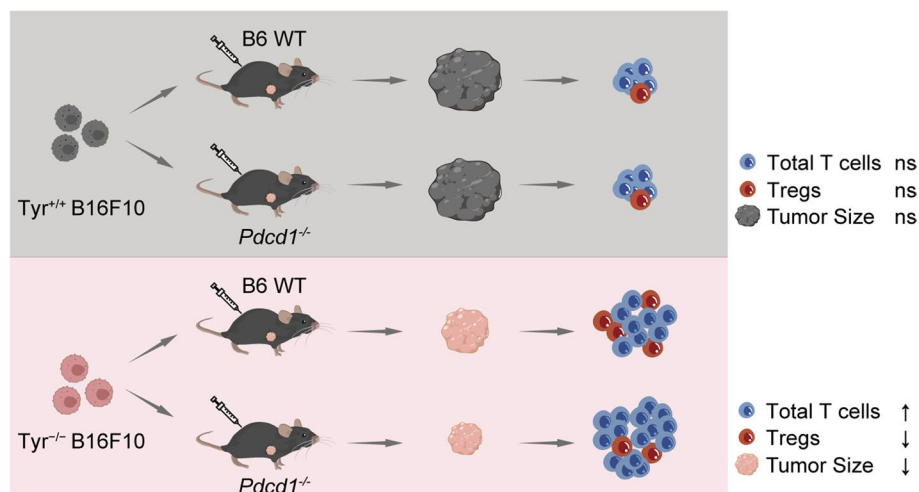


**Fig. 7** Schematic diagram. In tyrosinase-sufficient Tyr<sup>+/+</sup> tumors, *Pdcd1*<sup>-/-</sup> mice exhibit a tumor weight comparable to that of B6 WT mice. There are no significant changes in T-cell infiltration or Tregs expression in the tumors of either B6 WT or *Pdcd1*<sup>-/-</sup> mice. The absence of tyrosinase in B16 melanoma enhances the anti-tumor activity of PD-1 deficient T cells. In tyrosinase-deficient Tyr<sup>-/-</sup> tumor, the tumor weight is significantly reduced in *Pdcd1*<sup>-/-</sup> mice compared to the B6 WT controls. This reduction is associated with a significant increase in T-cell infiltration and a decrease in Treg frequencies in the *Pdcd1*<sup>-/-</sup> mice

blockade failed to reduce tumor weight (Additional file 1: Fig. S8A) or alter T cell infiltration (Additional file 1: Fig. S8B-F). Strikingly, in Tyr<sup>-/-</sup> tumors, PD-1 antibody treatment significantly suppressed tumor weight (Additional file 1: Fig. S9A), accompanied by increased T cell infiltration (Additional file 1: Fig. S9B), reduced CTLA-4 expression (Additional file 1: Fig. S9C-D), and decreased Foxp3<sup>+</sup> Tregs (Additional file 1: Fig. S9E). These data demonstrate that tyrosinase deficiency sensitizes melanoma to PD-1 blockade treatment.

## Discussion

Melanoma, a type of cancer arising from melanocytes, ranks among the most commonly diagnosed malignancies. Despite the success of immunotherapies targeting checkpoint molecules such as PD-1 in treating a part of melanoma patients, the phenomena of immune tolerance and resistance to immunotherapy warrant further investigations. In particular, the molecules expressed by cancer cells that suppress T cell responses remain only partially understood, highlighting the need for a deeper exploration into the molecular basis of these processes. Our analysis of TCGA data has revealed a significant link between increased Tyr expression in human melanoma and diminished overall survival rates. This finding implies that elevated levels of tyrosinase play a role in disease progression and a less favorable prognosis in melanoma. Despite this insight, the specific mechanisms through which tyrosinase influences cancer progression remain to be fully understood.

In our study, we investigated the influence of tyrosinase on melanoma progression and its modulation of the TME. By employing CRISPR/Cas9 to eliminate tyrosinase in B16-F10 melanoma cells, we observed a reduction in tumor growth, heightened T cell infiltration, increased expression of immune checkpoint molecules such as PD-1 and CTLA-4, and elevated levels of effector cytokines. Particularly notable was the synergistic effect of tyrosinase deficiency and PD-1 knockout, which boosted the anti-tumor immune response. Our findings highlight the immunomodulatory role of tyrosinase in melanoma by revealing that its deficiency unleashes the anti-tumor potential of PD-1 deficient T cells.

The TME within melanomas plays a critical role in disease progression, being categorized as either “cold” or “hot” based on T cell infiltration levels [25]. In our investigation, the ablation of tyrosinase in B16-F10 melanoma cells converted a “cold” tumor into a “hot” tumor, characterized by enhanced infiltration of CD4<sup>+</sup> and CD8<sup>+</sup> T cells, as confirmed through single-cell RNA sequencing and flow cytometry analyses. Furthermore, the deficiency of tyrosinase led to upregulation of the proinflammatory cytokines IFN- $\gamma$  and TNF- $\alpha$ , with Tbx21, a key transcription factor regulating IFN- $\gamma$  production [20], being upregulated in tyrosinase-deficient tumors, supported by q-PCR and single-cell RNA sequencing data. The heightened expression of these proinflammatory cytokines aids in the activation of effector immune responses [26], thereby facilitating the transition of immunologically “cold” tumors into “hot” tumors. NR4 A transcription factors, especially Nr4a1,

are crucial in inducing T cell exhaustion in cancers, especially in CD8<sup>+</sup> tumor-infiltrating lymphocytes in human melanoma where Nr4a1's expression correlates positively with PD-1 levels [18, 27]. Genetic research has pinpointed Nr4a1 as a pivotal driver of T cell dysfunction by boosting inhibitory receptors like PD-1 and influencing Treg development through enhanced Foxp3 expression [17, 28, 29]. Deletion of Nr4a1 and Nr4a2 has been shown to weaken the suppressive functions of tumor-infiltrating Tregs, highlighting the significance of NR4 A transcription factors in Treg-mediated immunosuppression within the TME [30]. Our study on tyrosinase-deficient tumors reveals heightened expression levels of PD-1 and Foxp3 in T cells. Using q-PCR and scRNA-seq analyses, we observed a significant upregulation of Nr4a1 within the TME. In this study, our findings demonstrate that tyrosinase-deficient melanoma exacerbates the expression of PD-1 and Tregs, potentially due to the increased of transcription factors like Nr4a1.

Our in vitro co-culture assays provide direct evidence that the presence of tyrosinase in melanoma suppresses T cell activation. This conclusion is further supported by the completely reversed cytokine profiles observed in Tyr KI co-cultures, which highlights the specificity of tyrosinase's function in this process. To consolidate our findings observed from tyrosinase deficient melanoma, we performed a genetic knock-in experiment to restore expression of tyrosinase on the background of Tyr deficient melanoma cells. Our results showed that restored expression of tyrosinase abolished the enhanced T cell activation in Tyr deficient cells, thereby confirming the specific role of tyrosinase in regulating T cell responses. It is noteworthy that future studies are valuable to extend these findings to models on diverse genetic backgrounds and human cellular models.

Previous research has demonstrated that melanogenesis can contribute to resistance to various therapies, including chemotherapy and radiotherapy, in human melanoma. While there is extensive knowledge on tyrosinase's involvement in melanin biosynthesis and melanoma susceptibility [31, 32], as well as the impact of the PD-1 pathway on T cell activation and exhaustion. The overall effect and relationship between tyrosine and PD-1 checkpoint inhibition immunotherapy have not been thoroughly investigated. Our research has revealed that the loss of tyrosinase in B16 melanoma enhances the anti-tumor potential of PD-1-deficient T cells, leading to 3.80-fold increase in tumor T cell infiltration and a substantial reduction in Treg frequencies in PD-1 knockout mice. The study introduces a novel discovery highlighting that tyrosinase deficiency can unleash the anti-tumor capabilities of *Pdcd1*<sup>-/-</sup> T cells, as evidenced by our

comparisons of T cell responses in *Pdcd1*<sup>-/-</sup> and WT mice bearing Tyr-deficient cells.

The in vivo PD-1 blockade experiments further validate the therapeutic potential of targeting tyrosinase. While PD-1 inhibition failed in WT tumors, its remarkable efficacy in Tyr<sup>-/-</sup> tumors demonstrates that tyrosinase deficiency converts immunologically "cold" melanomas into "hot" tumors responsive to checkpoint inhibition. This synergism mirrors clinical observations where combination therapies targeting tumor-intrinsic immunosuppressive pathways enhance immune checkpoint inhibitors efficacy [33]. Our data suggest that tyrosinase inhibitors could serve as adjuvants to overcome resistance in PD-1 blockade-refractory melanoma patients.

Our findings demonstrate that tyrosinase deficiency remodels the tumor microenvironment, converting "cold" melanomas into "hot" tumors responsive to PD-1 blockade. However, the clinical application of these results must consider the heterogeneity of melanoma subtypes. Notably, amelanotic melanomas, which lack pigmentation, are associated with increased aggressiveness and poorer prognoses compared to their pigmented counterparts. A recent spatial transcriptomic study of acral melanomas revealed distinct molecular characteristics in amelanotic tumors, including heightened translational reprogramming and immune evasion signatures [34]. These findings underscore the necessity of stratifying melanoma patients based on subtype-specific molecular profiles when developing combination therapies. Importantly, given the multifaceted roles tyrosinase may play beyond melanin synthesis, further exploration of its additional functions and mechanisms in the tumor microenvironment and immune regulation is warranted and could yield even more comprehensive insights for cancer therapy.

## Conclusions

These findings suggest that targeting tyrosinase could convert cold tumors into an immune-responsive state in vivo using murine models. Inhibiting tyrosinase could enhance the effectiveness of PD-1 blockade, offering a new approach for melanoma patients who fail in current PD-1 inhibitor treatment.

## Methods

### Animals

Female B6 mice aged 8 weeks were purchased from Beijing Vital River Laboratory Animal Technology Co., Ltd. *Pdcd1*<sup>-/-</sup> mice on the B6 background were prepared according to our previous study [21]. The mice were housed under specific pathogen-free conditions with free access to food and water. All animal procedures were performed in accordance with the guidelines approved

by the animal care committee at Xinxiang Medical University.

### Cell culture

Murine melanoma B16-F10 cells were obtained from the Cell Bank of the Chinese Academy of Sciences (Shanghai, China). B16-F10 cells were cultured in RPMI 1640 medium supplemented with 10% fetal bovine serum (FBS) and maintained in a humidified incubator at 37 °C with 5% CO<sub>2</sub>. When cell confluence reached approximately 80%, B16-F10 cells were detached using a trypsin-EDTA (0.25%) solution (Thermo Fisher Scientific) and collected.

### Generation of knockout cell lines

To generate gene-specific deletion using the CRISPR/Cas9 system, three sgRNAs targeting the *Tyr* gene were designed and cloned into the CRISPR-expression vectors pX458-DsRed2 and pX458-ECFP, which contained fluorescent reporters for single-cell sorting [35, 36]. The specific target site for the *Tyr* gene (Gene ID: ENSMUSG0000004651) was identified using the mouse genome database Ensembl (<http://asia.ensembl.org>). Using the online design software CRISPOR (<http://crisp.or.tefor.net/crispor.cgi>), three sgRNAs (sgRNA1:5'-CTG CCTGAA AGCTGGCCGCAGGG-3', sgRNA2:5'-CGG TCATCCACCCCTTTGAAGGG-3', sgRNA3:5'-CAA GAAATTCGAGAACTAACTGG-3') were designed and synthesized.

For transfection, a Neon<sup>®</sup> Transfection System (Thermo Fisher Scientific) electroporation instrument was used. B16-F10 cells were washed twice by PBS without Ca<sup>2+</sup> and Mg<sup>2+</sup>, then resuspended in Neon<sup>®</sup> Resuspension Buffer R. Plasmids containing the Cas9 nuclease and sgRNAs were introduced into cells, along with two fluorescent reporters (ECFP and DsRed2). The cell-DNA electroporation mixture was incubated at room temperature for 10 min before being transferred to a 10 µL Neon<sup>®</sup> tip. Electroporation of B16-F10 cells was performed using the following conditions: 1400 V/20 ms/2 pulses. Post-electroporation, cells expressing both fluorescent proteins were sorted using a BD FACSAria<sup>™</sup> Fusion flow cytometer and plated in individual wells for isolation. PCR amplification of each sorted single cell was performed to confirm successful gene editing, and the resulting PCR products were subsequently subjected to Sanger sequencing for analysis.

### Generation of *Tyr* knock-in in *Tyr*-deficient B16-F10 melanoma cells

To generate a gene knock-in at the *Rosa26* safe harbor locus, the mouse *Tyr* coding sequence (ENS-MUST0000004770.7) was amplified using B16-F10

cDNA as a PCR template. The amplified sequence was then cloned into the targeting vector pKR26-iBFP using the NEBuilder HiFi DNA Assembly Master Mix (New England Biolabs). The resulting plasmid was utilized as a template for homologous recombination to create a knock-in cell line expressing both the *Tyr* protein and a BFP fluorescent reporter. The plasmids were subsequently transfected into *Tyr*-deficient B16-F10 melanoma cells using the Neon<sup>®</sup> Transfection System (Thermo Fisher Scientific), following established protocols from previous studies [35, 37]. The Transfection cells were then sorted and profiled as described before [36, 38]. All the proliferated cells were screened for BFP expression by flow cytometry to confirm successful recombination.

### Melanoma cells and T-cell co-culture assay

T cells were isolated from mouse lymph nodes using the Dynabeads<sup>™</sup> Untouched<sup>™</sup> Mouse T Cells Kit (Thermo Fisher Scientific). These isolated T cells were then seeded into 6-well plates that had been pre-coated with anti-CD3 monoclonal antibody (1 µg/mL, eBioscience), along with soluble anti-CD28 monoclonal antibody (1 µg/mL, eBioscience) and 10 ng/mL of mouse interleukin-2 (IL-2, PEPROTech). The T cells were cultured for an additional 3 days to achieve activation before further experimentation. Following activation, the stimulated T cells were harvested and co-cultured with WT, *Tyr* KO, and *Tyr* KI B16-F10 melanoma cell lines at a 2:1 ratio for 4 h. The relative expression levels of *Tbx21*, *Nr4a1*, *TNF-α* and *IFN-γ* mRNA in the cells were assessed using q-PCR assays.

### Tumor graft

Tumors were established in 8- to 10-week-old mice through subcutaneous injection. Each mouse received an injection of  $2.0 \times 10^5$  B16-F10 cells suspended in 100 µL of sterile PBS in the right flank. Tumor volume was measured by recording the length and width every 2 to 3 days starting on day 6, using a digital caliper to record length and width. Volume was calculated using the formula  $l/2 \cdot w^2$ ,  $l$  represents the length and  $w$  represents the width. At the endpoint of the experiments, the mice were euthanized using CO<sub>2</sub>. Subcutaneous tumors were then surgically excised and weighed.

### In vivo treatment with anti-PD-1 antibody

For in vivo cancer therapy, 100 µg of anti-mouse PD-1 monoclonal antibody (RMP1-14, BioXCell) or an IgG2a isotype control (BioXCell) was administered intraperitoneally every 2 days following tumor injection.

### Immune cell extraction

Tumors were minced and digested in RPMI1640 medium containing 0.8 mg/mL Collagenase IV (Sigma), 0.2 mg/mL DNase I (Sigma), and 10% FBS for 30 min at 37 °C with gentle agitation. The resulting cell suspensions were passed through 70 μm nylon cell strainers, collected by centrifugation, and resuspended in FACS buffer (1 × PBS, pH 7.4, 2 mM EDTA, pH 8.0, 1% FBS).

### Flow cytometry and antibodies

For flow cytometry analysis, cells isolated from the tumors were stained using a standard protocol as described in previous studies [39, 40]. Single-cell suspensions were incubated with 2.4G2 antibody for Fc receptor blocking at 4°C for 20 min, followed by a 30-min incubation with the specified antibodies (Additional file 2: Table S1) at 4 °C. The stained cells were then acquired using a FACS Canto flow cytometer (BD Biosciences), and FACS analyses were performed using FlowJo 10.0 software.

### Single-cell RNA sequencing

For scRNA-seq analysis of tumor-infiltrating immune cells (TIICs), WT and *Tyr* knockout B16-F10 melanoma cells were implanted in the right flank of female C57BL/6 mice ( $n = 3$ ). At the endpoint, the tumors were dissected from the surrounding fascia, and single cell suspensions were prepared from both the *Tyr* knockout and the WT melanoma cells. TIICs were isolated using the FACSARIA II cell sorter (BD Biosciences, USA) and stained with anti-mouse CD45.2 PE-Cy7 (eBioscience). CD45<sup>+</sup> TIICs were labeled with the BD Single-Cell Multiplexing Kit (BD Biosciences) according to the manufacturer's protocol. Cells from each group were labeled with sample tags, washed, and pooled. The pooled sample was then counted, resuspended, and subjected to single-cell capture and cDNA Synthesis using the BD Rhapsody Express Single-Cell Analysis System (BD Biosciences). cDNA libraries were prepared using the mRNA Targeted and Sample Tag Library preparation method along with the BD Rhapsody Targeted mRNA Amplification and BD Single-Cell Multiplexing Kits and protocols from BD Biosciences. The libraries were sequenced on the Illumina NovaSeq platform (Novogene), and clustering analysis and high-dimensional visualization were performed using the SeqGeq™ software.

### Quantitative real-time PCR

Total RNA was extracted from tumors using the TaKaRa MiniBEST Universal RNA Extraction Kit (Takara) according to the manufacturer's instructions. The extracted RNA was reverse-transcribed into cDNA using the

RevertAid First Strand cDNA Synthesis Kit (Thermo Fisher Scientific). q-PCR was performed on the ABI PRISM 7500 Fast Real-Time PCR System (Applied Biosystems, USA) with TB Green Premix Ex Taq (Takara). The expression levels of individual genes were normalized to GAPDH expression, with fold changes between samples determined using the  $2^{-\Delta\Delta C_t}$  method. Sequences for the q-PCR primers can be found in Additional file 2: Table S2.

### Analysis of TCGA data and overall survival data

Gene expression data for SKCM patients from TCGA were accessed via the website (<http://gepia2.cancer-pku.cn>) [41]. *Tyr* mRNA levels in normal tissue and SKCM tumor tissues were generated using GEPIA2 online software. Survival analysis was performed using the same tool.

### Statistical analysis

Statistical analyses were performed using GraphPad Prism software version 9.0. Student's *t*-test was used for comparing two groups. One-way ANOVA was used when comparing several groups vs control.  $p < 0.05$  values were considered significant. The statistical details of experiments can be found in the figure legends.

### Abbreviations

Tyr	Tyrosinase
TME	Tumor microenvironment
KO	Knockout
scRNA-seq	Single-cell RNA sequencing
Treg	Regulatory T cell
TCGA	The Cancer Genome Atlas
SKCM	Skin Cutaneous Melanoma
sgRNAs	Single guide RNAs
WT	Wild-type
B6	C57BL/6
q-PCR	Quantitative real-time PCR
KI	Knock-in
FBS	Fetal bovine serum
TIICs	Tumor-infiltrating immune cells

### Supplementary Information

The online version contains supplementary material available at <https://doi.org/10.1186/s12915-025-02237-4>.

Additional file 1: Fig. S1-10. Fig. S1. Mutated sequences encompassing the site targeted by the CRISPR/Cas9 in the *Tyr* KO B16-F10 cell clones. Fig. S2. Sorting of CD45<sup>+</sup> tumor-infiltrating immune cells from the single cell suspension. Fig. S3. Heatmap of the marker gene expression across fourteen clusters of tumor-infiltrating cell subsets based on scRNA-seq data. Fig. S4. CRISPR/Cas9-mediated *Tyr* knock-in rescues melanogenic function in *Tyr*-deficient B16-F10 melanoma cells. Fig. S5. Tyrosinase genetic modifications in melanoma cells differentially regulate T cell activation markers during co-culture. Fig. S6. Quantification of CD45<sup>+</sup> cells, CD4<sup>+</sup> T cells, CD8<sup>+</sup> T cells per gram of tumor in *Tyr*<sup>+/+</sup> B16-F10 tumors from *Pdcd1*<sup>-/-</sup> and B6 mice. Fig. S7. Quantification of CD4<sup>+</sup> T cells, CD8<sup>+</sup> T cells per gram of tumor in *Tyr*<sup>-/-</sup> B16-F10 tumors from *Pdcd1*<sup>-/-</sup> and B6 mice. Fig. S8. The impact of PD-1 blockade treatment on tumor growth and T cells in *Tyr*<sup>+/+</sup> B16-F10

tumors. Fig S9. Data are presented as mean  $\pm$  SEM ( $\alpha$ -PD-1 treated mice, n=5; Iso-Ctrl treated mice, n=8). Fig S10. Uncropped gel image.

Additional file 2: Table S1. Antibodies used for flow cytometric analysis. Table S2. The sequences of the primers for q-PCR.

### Acknowledgements

We acknowledge the Laboratory of Genetic Regulators in the Immune System (GRIS) animal facility and flow cytometry platform for technical support.

### Authors' contributions

LZ and YL designed the project and wrote the manuscript. RH, YW, HT, MX and KH performed the experiments and analyzed the data. YS, GG and XF were involved in experiments of cell line genetic engineering and mouse immunophenotyping. TL and BZ performed the analysis of scRNA-seq data. MB, TL and LL participated in writing and revising the manuscript. All authors read and approved the final manuscript.

### Funding

This work was supported by National Natural Science Foundation of China under Grants [32170879] to LZ, [81901581] to RH, and [32070898] to YL. This work was supported by grants from Science and Technology Innovation Program of Hunan Province [2023DK2005] [2024RC1071] [2022 WZ1021] and [2022RC1223]. The animal model generation and housing were also supported by 111 program [D20036] and Zhongyuan Academician Fund from Henan Province C24185.

### Data availability

TCGA-SKCM dataset was analyzed using GEPIA2 web server URL: <http://gepia2.cancer-pku.cn> [41]. scRNA-seq data generated in this study was deposited in the NCBI's Gene Expression Omnibus (GEO GSE273734). URL: <https://www.ncbi.nlm.nih.gov/geo/query/acc.cgi?acc=GSE273734>. All other data that support the findings of this study are available from the corresponding author upon reasonable request.

### Declarations

#### Ethics approval and consent to participate

All institutional and national guidelines for the care and use of laboratory animals were followed. The procedures were conducted according to the Standard of Laboratory Animals—General Code of Animal Welfare (GB/T 42011 – 2022) and approved by the animal care committee at Xixiang Medical University.

#### Consent for publication

Not applicable.

#### Competing interests

The authors declare no competing interests.

Received: 23 August 2024 Accepted: 6 May 2025

Published online: 15 May 2025

### References

1. Brozyna AA, Jozwicki W, Carlson JA, Slominski AT. Melanogenesis affects overall and disease-free survival in patients with stage III and IV melanoma. *Hum Pathol.* 2013;44(10):2071–4.
2. Bishop DT, Demenais F, Iles MM, Harland M, Taylor JC, Corda E, et al. Genome-wide association study identifies three loci associated with melanoma risk. *Nat Genet.* 2009;41(8):920–5.
3. Pelayo BA, Fu YM, Meadows GG. Decreased tissue plasminogen activator and increased plasminogen activator inhibitors and increased activator protein-1 and specific promoter 1 are associated with inhibition of invasion in human A375 melanoma deprived of tyrosine and phenylalanine. *Int J Oncol.* 2001;18(4):877–83.
4. Pelayo BA, Fu YM, Meadows GG. Inhibition of B16BL6 melanoma invasion by tyrosine and phenylalanine deprivation is associated with decreased secretion of plasminogen activators and increased plasminogen activator inhibitors. *Clin Exp Metastasis.* 1999;17(10):841–8.
5. Fu YM, Yu ZX, Pelayo BA, Ferrans VJ, Meadows GG. Focal adhesion kinase-dependent apoptosis of melanoma induced by tyrosine and phenylalanine deficiency. *Cancer Res.* 1999;59(3):758–65.
6. Wolchok JD, Chiarion-Sileni V, Gonzalez R, Rutkowski P, Grob JJ, Cowey CL, et al. Overall Survival with Combined Nivolumab and Ipilimumab in Advanced Melanoma. *N Engl J Med.* 2017;377(14):1345–56.
7. Larkin J, Chiarion-Sileni V, Gonzalez R, Grob JJ, Rutkowski P, Lao CD, et al. Five-Year Survival with Combined Nivolumab and Ipilimumab in Advanced Melanoma. *N Engl J Med.* 2019;381(16):1535–46.
8. He X, Xu C. Immune checkpoint signaling and cancer immunotherapy. *Cell Res.* 2020;30(8):660–9.
9. Chamoto K, Yaguchi T, Tajima M, Honjo T. Insights from a 30-year journey: function, regulation and therapeutic modulation of PD1. *Nat Rev Immunol.* 2023;23(10):682–95.
10. Sullivan RJ, Flaherty KT. Immunotherapy: Anti-PD-1 therapies—a new first-line option in advanced melanoma. *Nat Rev Clin Oncol.* 2015;12(11):625–6.
11. Robert C, Schachter J, Long GV, Arance A, Grob JJ, Mortier L, et al. Pembrolizumab versus Ipilimumab in Advanced Melanoma. *N Engl J Med.* 2015;372(26):2521–32.
12. Hegde PS, Chen DS. Top 10 Challenges in Cancer Immunotherapy. *Immunity.* 2020;52(1):17–35.
13. Gladfelter P, Darwish NHE, Mousa SA. Current status and future direction in the management of malignant melanoma. *Melanoma Res.* 2017;27(5):403–10.
14. Spranger S, Spaapen RM, Zha Y, Williams J, Meng Y, Ha TT, et al. Up-regulation of PD-L1, IDO, and T(regs) in the melanoma tumor microenvironment is driven by CD8(+) T cells. *Sci Transl Med.* 2013;5(200):200ra116.
15. Ribas A, Robert C, Hodi FS, Wolchok JD, Hwu WJ. Association of response to programmed death receptor 1 (PD-1) blockade with pembrolizumab (MK-3475) with an interferon-inflammatory immune gene signature. *J Clin Oncol.* 2015;33(2):141–7.
16. Hearing VJ, Tsukamoto K. Enzymatic control of pigmentation in mammals. *FASEB J.* 1991;5(14):2902–9.
17. Liu X, Wang Y, Lu H, Li J, Yan X, Xiao M, et al. Genome-wide analysis identifies NR4A1 as a key mediator of T cell dysfunction. *Nature.* 2019;567(7749):525–9.
18. Chen J, Lopez-Moyado IF, Seo H, Lio CJ, Hempleman LJ, Sekiya T, et al. NR4A transcription factors limit CAR T cell function in solid tumours. *Nature.* 2019;567(7749):530–4.
19. Shen J, Xiao Z, Zhao Q, Li M, Wu X, Zhang L, et al. Anti-cancer therapy with TNFalpha and IFNgamma: A comprehensive review. *Cell Prolif.* 2018;51(4):e12441.
20. Szabo SJ, Kim ST, Costa GL, Zhang X, Fathman CG, Glimcher LH. A novel transcription factor, T-bet, directs Th1 lineage commitment. *Cell.* 2000;100(6):655–69.
21. Lu L, Li T, Feng X, Liu Z, Liu Y, Chao T, et al. Excessive immunosuppression by regulatory T cells antagonizes T cell response to schistosome infection in PD-1-deficient mice. *PLoS Pathog.* 2022;18(6):e1010596.
22. Iwai Y, Ishida M, Tanaka Y, Okazaki T, Honjo T, Minato N. Involvement of PD-L1 on tumor cells in the escape from host immune system and tumor immunotherapy by PD-L1 blockade. *Proc Natl Acad Sci U S A.* 2002;99(19):12293–7.
23. Iwai Y, Terawaki S, Honjo T. PD-1 blockade inhibits hematogenous spread of poorly immunogenic tumor cells by enhanced recruitment of effector T cells. *Int Immunol.* 2005;17(2):133–44.
24. Curran MA, Montalvo W, Yagita H, Allison JP. PD-1 and CTLA-4 combination blockade expands infiltrating T cells and reduces regulatory T and myeloid cells within B16 melanoma tumors. *Proc Natl Acad Sci U S A.* 2010;107(9):4275–80.
25. Gajewski TF. The Next Hurdle in Cancer Immunotherapy: Overcoming the Non-T-Cell-Inflamed Tumor Microenvironment. *Semin Oncol.* 2015;42(4):663–71.
26. Zheng X, Wu Y, Bi J, Huang Y, Cheng Y, Li Y, et al. The use of supercytokines, immunocytokines, engager cytokines, and other synthetic cytokines in immunotherapy. *Cell Mol Immunol.* 2022;19(2):192–209.

27. Tirosh I, Izar B, Prakadan SM, Wadsworth MH 2nd, Treacy D, Trombetta JJ, et al. Dissecting the multicellular ecosystem of metastatic melanoma by single-cell RNA-seq. *Science*. 2016;352(6282):189–96.
28. Sekiya T, Kashiwagi I, Yoshida R, Fukaya T, Morita R, Kimura A, et al. Nr4a receptors are essential for thymic regulatory T cell development and immune homeostasis. *Nat Immunol*. 2013;14(3):230–7.
29. Sekiya T, Kondo T, Shichita T, Morita R, Ichinose H, Yoshimura A. Suppression of Th2 and Tfh immune reactions by Nr4a receptors in mature T reg cells. *J Exp Med*. 2015;212(10):1623–40.
30. Hibino S, Chikuma S, Kondo T, Ito M, Nakatsukasa H, Omata-Mise S, et al. Inhibition of Nr4a Receptors Enhances Antitumor Immunity by Breaking Treg-Mediated Immune Tolerance. *Cancer Res*. 2018;78(11):3027–40.
31. Jimbow K, Iwashina T, Alena F, Yamada K, Pankovich J, Umemura T. Exploitation of pigment biosynthesis pathway as a selective chemotherapeutic approach for malignant melanoma. *J Invest Dermatol*. 1993;100(2 Suppl):231S–S238.
32. Law MH, Bishop DT, Lee JE, Brossard M, Martin NG, Moses EK, et al. Genome-wide meta-analysis identifies five new susceptibility loci for cutaneous malignant melanoma. *Nat Genet*. 2015;47(9):987–95.
33. Alsaafeen BH, Ali BR, Elkord E. Resistance mechanisms to immune checkpoint inhibitors: updated insights. *Mol Cancer*. 2025;24(1):20.
34. McMahan M, Deacon DC. Spatial sequencing reveals transcriptional variation between amelanotic and pigmented acral melanoma. *Br J Dermatol*. 2024;191(4):483–4.
35. Luo J, Lu L, Gu Y, Huang R, Gui L, Li S, et al. Speed genome editing by transient CRISPR/Cas9 targeting and large DNA fragment deletion. *J Biotechnol*. 2018;281:11–20.
36. Huang R, Guo G, Lu L, Fu R, Luo J, Liu Z, et al. The three members of the Vav family proteins form complexes that concur to foam cell formation and atherosclerosis. *J Lipid Res*. 2019;60(12):2006–19.
37. Zhang L, Huang R, Lu L, Fu R, Guo G, Gu Y, et al. Gene Knock-in by CRISPR/Cas9 and Cell Sorting in Macrophage and T Cell Lines. *Journal of visualized experiments. JoVE*. 2021;(177):e62328.
38. Zhang L, Feng X, Shen Y, Wang Y, Liu Z, Ma Y, et al. A novel ZsGreen knock-in melanoma cell line reveals the function of CD11b in tumor phagocytosis. *Immunol Cell Biol*. 2022;100(9):691–704.
39. Chao T, Lu L, Zhang L, Huang R, Liu Z, Zhou B, et al. An inducible model for specific neutrophil depletion by diphtheria toxin in mice. *Sci China Life Sci*. 2021;64(8):1227–35.
40. Ghislat G, Cheema AS, Baudoin E, Verthuy C, Ballester PJ, Crozat K, et al. NF-kappaB-dependent IRF1 activation programs cDC1 dendritic cells to drive antitumor immunity. *Sci Immunol*. 2021;6(61):eabg3570.
41. Tang Z, Kang B, Li C, Chen T, Zhang Z. GEPIA2: an enhanced web server for large-scale expression profiling and interactive analysis. *Nucleic Acids Res*. 2019;47(W1):W556–60.

## Publisher's Note

Springer Nature remains neutral with regard to jurisdictional claims in published maps and institutional affiliations.